

Plasmonics: the next chip-scale technology

The development of chip-scale electronics and photonics has led to remarkable data processing and transport capabilities that permeate almost every facet of our lives. Plasmonics is an exciting new device technology that has recently emerged. It exploits the unique optical properties of metallic nanostructures to enable routing and manipulation of light at the nanoscale. A tremendous synergy can be attained by integrating plasmonic, electronic, and conventional dielectric photonic devices on the same chip and taking advantage of the strengths of each technology.

Rashid Zia, Jon A. Schuller, Anu Chandran, and Mark L. Brongersma*

Geballe Laboratory for Advanced Materials, Stanford University, Stanford, CA 94305 USA

**E-mail: brongersma@stanford.edu*

The ever-increasing demand for faster information transport and processing capabilities is undeniable. Our data-hungry society has driven enormous progress in the Si electronics industry and we have witnessed a continuous progression towards smaller, faster, and more efficient electronic devices over the last five decades. The scaling of these devices has also brought about a myriad of challenges. Currently, two of the most daunting problems preventing significant increases in processor speed are thermal and signal delay issues associated with electronic interconnection¹⁻³. Optical interconnects, on the other hand, possess an almost unimaginably large data carrying capacity, and may offer interesting new solutions for circumventing these problems^{4,5}. Optical alternatives may be particularly attractive for future chips with more distributed architectures in which a multitude of fast electronic computing units (cores) need to be connected by high-speed links. Unfortunately, their implementation is hampered by the large size mismatch between

electronic and dielectric photonic components. Dielectric photonic devices are limited in size by the fundamental laws of diffraction to about half a wavelength of light and tend to be at least one or two orders of magnitude larger than their nanoscale electronic counterparts. This obvious size mismatch between electronic and photonic components presents a major challenge for interfacing these technologies. Further progress will require the development of a radically new chip-scale device technology that can facilitate information transport between nanoscale devices at optical frequencies and bridge the gap between the world of nanoscale electronics and microscale photonics.

We discuss a candidate technology that has recently emerged^{6,7} and has been termed 'plasmonics'⁸. This device technology exploits the unique optical properties of nanoscale metallic structures to route and manipulate light at the nanoscale. By integrating plasmonic, electronic, and conventional photonic devices on the same chip, it would be possible to take advantage of the strengths of each technology. We

present some of our recent studies on plasmonic structures and conclude by providing an assessment of the potential opportunities and limitations for Si chip-scale plasmonics.

Plasmonics as a new device technology

Metal nanostructures may possess exactly the right combination of electronic and optical properties to tackle the issues outlined above and realize the dream of significantly faster processing speeds. The metals commonly used in electrical interconnection such as Cu and Al allow the excitation of surface plasmon-polaritons (SPPs). SPPs are electromagnetic waves that propagate along a metal-dielectric interface and are coupled to the free electrons in the metal (Fig. 1)⁹⁻¹¹.

From an engineering standpoint, an SPP can be viewed as a special type of light wave. The metallic interconnects that support such waves thus serve as tiny optical waveguides termed plasmonic waveguides. The notion that the optical mode ('light beam') diameter normal to the metal interface can be significantly smaller than the wavelength of light¹² has generated significant excitement and sparked the dream that one day we will be able to interface nanoscale electronics with similarly sized optical (plasmonic) devices.

It is important to realize that, with the latest advances in electromagnetic simulations and current complementary metal-oxide semiconductor (CMOS)-compatible fabrication techniques, a variety of functional plasmonic structures can be designed and fabricated in a Si foundry right now. Current Si-based integrated circuit technology already uses nanoscale metallic structures, such as Cu and Al interconnects, to route electronic signals between transistors on a chip. This mature processing technology can thus be used to our advantage in integrating plasmonic devices with their electronic and dielectric photonic counterparts. In some cases, plasmonic waveguides may even perform a dual function and simultaneously carry both optical and electrical signals, giving rise to exciting new capabilities¹³.

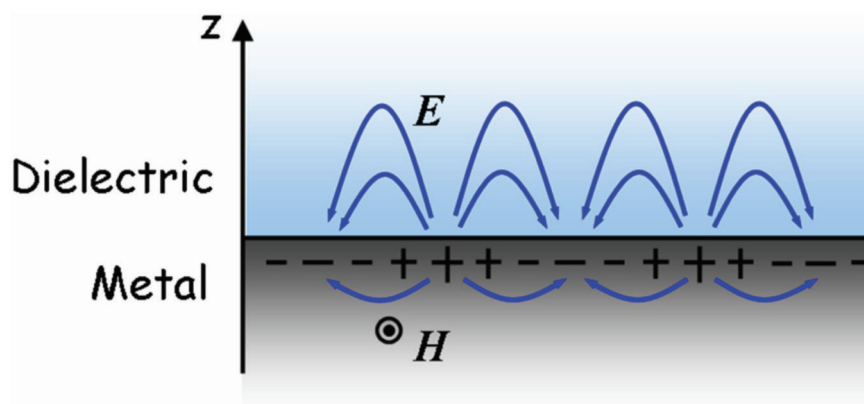


Fig. 1 An SPP propagating along a metal-dielectric interface. These waves are transverse magnetic in nature. Their electromagnetic field intensity is highest at the surface and decays exponentially away from the interface. From an engineering standpoint, an SPP can be viewed as a special type of light wave propagating along the metal surface.

Imaging SPPs with a photon scanning tunneling microscope

In order to study the propagation of SPPs, we constructed a photon scanning tunneling microscope (PSTM)¹⁴ by modifying a commercially available scanning near-field optical microscope. PSTM is the tool of choice for characterizing SPP propagation along extended films as well as metal stripe waveguides¹⁵⁻¹⁷. Fig. 2a shows how a microscope objective at the heart of our PSTM can be used to focus a laser beam onto a metal film at a well-defined angle and thereby launch an SPP along the top metal surface. This method of exciting SPPs makes use of the well-known Kretschmann geometry that enables phase matching of the free space excitation beam and the SPP¹⁸.

A sharp, metal-coated pyramidal tip (Figs. 2b and 2c) is used to tap into the guided SPP wave locally and scatter light toward a far-field detector. These particular tips have a nanoscale aperture at the top of the pyramid through which light can be collected. The scattered light is then detected with a photomultiplier tube. The signal provides a measure of the local light intensity right underneath the tip and, by scanning the tip over the metal surface, the propagation of SPPs can be imaged.

The operation of the PSTM can be illustrated by investigating the propagation of SPPs on a patterned Au film (Fig. 2d). Here, a focused ion beam (FIB) was used to define a series of parallel grooves, which serve as a Bragg grating to reflect SPP waves. Fig. 2e shows a PSTM image of an SPP wave excited with a 780 nm wavelength laser and directed toward the Bragg grating. The back reflection of the SPP from the grating results in the standing wave interference pattern observed in the image. From this type of experiment the wavelength of SPPs can be determined in a straightforward manner and compared to theory.

The PSTM can also be used to image SPP propagation directly in plasmonic structures and devices of more complex architecture to determine their behavior. This is quite different from typical

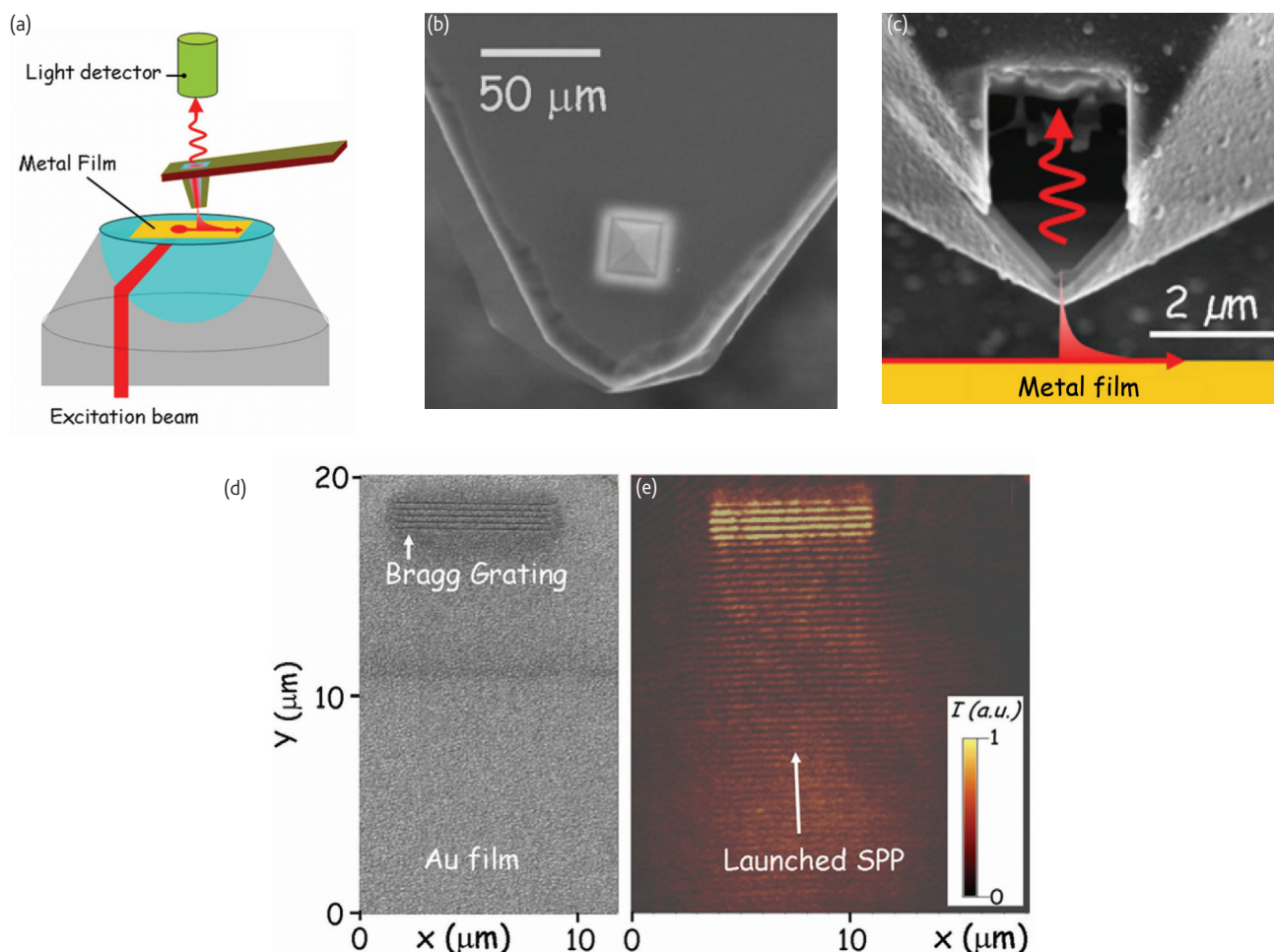


Fig. 2 (a) Schematic of the operation of a PSTM that enables the study of SPP propagation along metal film surfaces. The red arrow shows how an SPP is launched from an excitation spot onto a metal film surface using a high numerical aperture microscope objective. (b) Scanning electron microscopy (SEM) image of the near-field optical cantilever probe used in our experiments. The tip consists of a microfabricated, hollow glass pyramid coated with an optically thick layer of Al. Light can be collected or emitted through a ~ 50 nm hole fabricated in the Al film on the top of the pyramid. (c) A cross-sectional view of the same hollow pyramidal tip after a large section was cut out of the sidewall with a focused ion beam (FIB). In close proximity to the surface, the pyramidal tip can tap into the propagating SPP and scatter out a little bit of light through the ~ 50 nm hole (shown pictorially). The scattered light is detected in the far-field, providing a measure of the local field intensity right underneath the tip. By scanning the tip over the sample and measuring the intensity at each tip position, images of propagating SPPs can be created. (d) SEM image of a Au film into which a Bragg grating has been fabricated using a FIB. (e) PSTM image of an SPP wave launched along the metal film toward the Bragg grating. The back reflection of the SPP from the Bragg grating results in the observation of a standing wave interference pattern.

characterization procedures for photonic devices in which the device is seen as a black box with input and output ports. In such cases, the device operation is inferred from responses measured at output ports to different stimuli provided at the input ports. The PSTM provides a clear advantage by providing a direct method to observe the inner workings of plasmonic devices, offering a peek inside the box.

Experiments and simulations on plasmonic waveguides

The valuable information about plasmonic structures provided by PSTM measurements allows us to evaluate the utility of plasmonics for interconnection. Plasmonic stripe waveguides provide a natural starting

point for this discussion as such stripes very closely resemble conventional metal interconnects.

Electron beam lithography has been used to generate 55 nm thick Au stripes on a SiO₂ glass slide with stripe widths ranging from 5 μ m to 50 nm. Au stripes are ideal for fundamental waveguide transport studies as they are easy to fabricate, do not oxidize, and exhibit a qualitatively similar plasmonic response to Cu and Al¹⁹. Fig. 3a shows an optical micrograph of a typical device consisting of a large Au area from which SPPs can be launched onto varying width metal stripes. An scanning electron microscopy (SEM) image of a 250 nm wide stripe is shown as an inset. The red arrow shows how light is launched from a focused laser spot into a 1 μ m wide stripe.

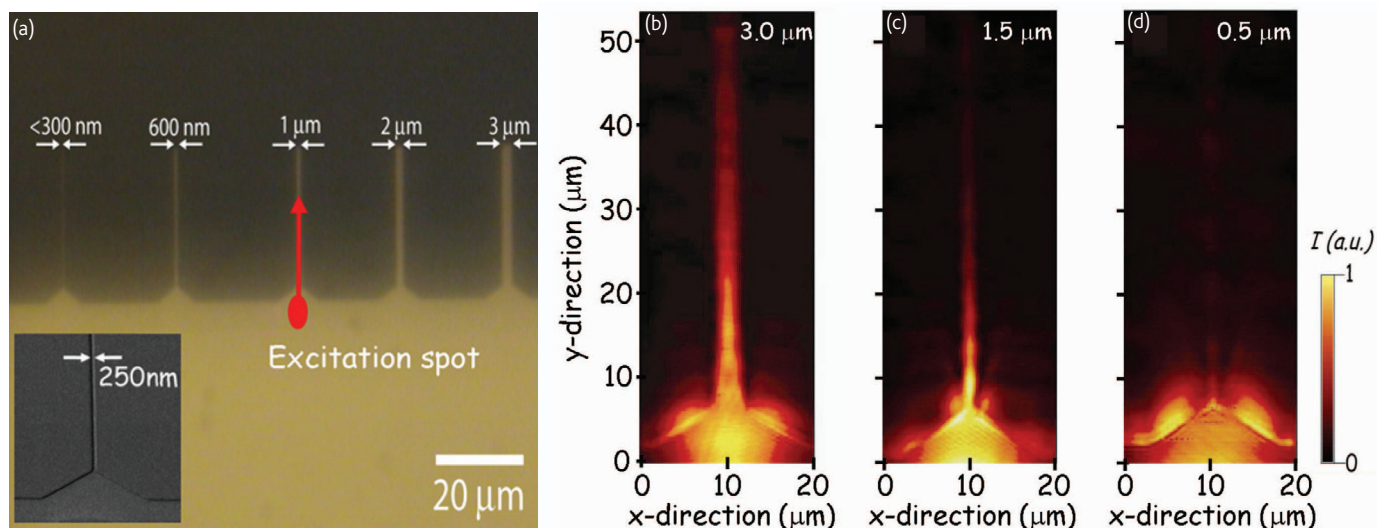


Fig. 3 (a) Optical microscopy image of a SiO_2 substrate with an array of Au stripes attached to a large launchpad generated by electron beam lithography. The red arrow illustrates the launching of an SPP into a $1\text{ }\mu\text{m}$ wide stripe. (b, c, and d) PSTM images of SPPs excited at $\lambda = 780\text{ nm}$ and propagating along $3.0\text{ }\mu\text{m}$, $1.5\text{ }\mu\text{m}$, and $0.5\text{ }\mu\text{m}$ wide Au stripes, respectively. (Parts b, c, and d reprinted with permission from²³. © American Physical Society.)

Figs. 3b, 3c, and 3d show PSTM images of SPPs excited at $\lambda = 780\text{ nm}$ and propagating along $3.0\text{ }\mu\text{m}$, $1.5\text{ }\mu\text{m}$, and $0.5\text{ }\mu\text{m}$ wide Au stripes, respectively. The $3.0\text{ }\mu\text{m}$ wide stripe can be used to propagate signals over several tens of microns. Similar to previous far-field measurements along Ag stripes²⁰, it is clear that the propagation distance of SPPs decreases with decreasing stripe width. A better understanding of this behavior can be obtained from full-field simulations and a recently developed, intuitive ray optics picture for plasmon waveguides²¹⁻²³. A selection of these simulation results is presented next, followed by a discussion of the potential uses for these relatively short propagation distance waveguides.

Recent numerical work has demonstrated that the modal solutions of plasmonic stripe waveguides are hybrid transverse electric-transverse magnetic (TE-TM) modes, and therefore their analysis requires

numerical solution of the full vectorial wave equation²⁴⁻²⁶. To this end we have developed a full vectorial magnetic field, finite difference method (FVH-FDM) for solving the electromagnetic Helmholtz equation^{21,27}. This is a frequency domain method and has clear advantages over the very popular finite difference time domain methods. One particularly attractive feature is that realistic, frequency-dependent dielectric constants for metals and dielectrics can be used as inputs to the simulation.

Fig. 4 shows two modal solutions obtained with this method for a 55 nm thick and $3.5\text{ }\mu\text{m}$ wide Au stripe on glass at $\lambda = 800\text{ nm}$. It is worth noticing that SPP modes are supported on both the top and bottom Au surfaces. These waves can simultaneously carry information without interacting. The mode propagating along the top metal/air interface is called a 'leaky' mode and the mode at the bottom

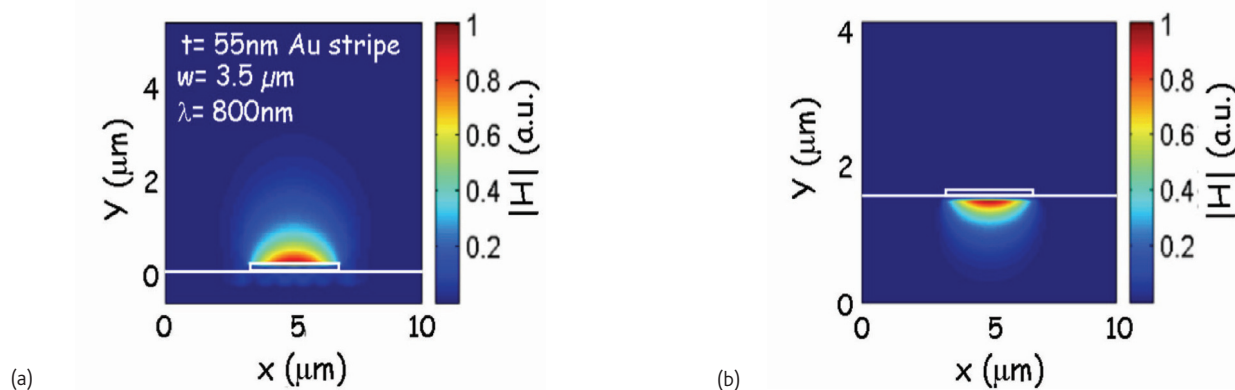


Fig. 4 Simulated SPP mode profiles for a 55 nm thick and $3.5\text{ }\mu\text{m}$ wide Au stripe on a SiO_2 glass substrate. It shows the fundamental leaky (left) and bound (right) SPP modes propagating at the top air/metal and bottom glass/metal interfaces, respectively. Both modes can be employed simultaneously for information transport. (Reprinted with permission from²¹. © 2005 American Physical Society.)

metal/glass interface is called a 'bound' mode. The fields associated with these modes have a large H_x component, which is reminiscent of the purely TM nature of SPP modes on infinite metal films. For this reason they are often called quasi-TM modes.

In addition to calculating the field-intensity distributions of SPP modes, the FVH-FDM also provides values for the real and imaginary parts of the propagation constants. Fig. 5 shows the complex propagation constants ($\beta_{sp} + i\alpha_{sp}$) determined for the lowest order leaky, quasi-TM modes supported by 55 nm thick Au stripes of various widths W at an excitation wavelength of 800 nm²¹. The inset in the bottom graph shows the geometry used in the simulations. For this simulation, the dielectric properties of Au ($\epsilon_{Au} = -26.1437 + 1.8497i$) at the excitation wavelength of $\lambda = 800$ nm were used²⁸.

Several important trends can be discerned from these plots. Similar to dielectric waveguides, larger structures tend to support an increased number of modes. Higher-order SPP modes exhibit a higher number of maxima in the transverse magnetic field H_x along the x -direction. As the stripe width is decreased to a couple of times the excitation wavelength, the wave number β_{sp} for all modes starts to decrease from the value of an infinitely wide stripe ($\beta_{sp} = 1.02$). The decrease of the propagation constant with decreasing stripe width first results in a reduced confinement of the modes and finally cutoff occurs for a width of ~ 1.3 μm . At this width, the SPP propagation constant has become equal to the propagation constant in air, β_0 . The diminished confinement for narrow stripes results in a concomitant increase in the radiation losses into the high-index SiO_2 substrate. This explains the

larger α_{sp} observed for small stripe widths. The 0.5 μm wide waveguide in Fig. 3 is below the cutoff and does not support a quasi-TM mode. It appears, however, that there is a finite propagation length, which can be explained by taking into account the contribution to the measured field intensity from the radiation continuum (i.e. nonguided waves)²³. It is important to note that simulations also predict a cutoff for the bound modes, albeit at a slightly narrower stripe width²¹.

This type of knowledge presented on the propagation behavior of plasmonic interconnects (mode size, propagation length, and cutoff) is essential for chip-designers and process engineers. It is clear that the short propagation distances found for plasmonic waveguides preclude direct competition with low-loss dielectric waveguide components. However, plasmonic structures can add new types of functionality to chips that cannot be obtained with dielectric photonics. One category of structures offering unique capabilities is active plasmonic interconnects. Such interconnects may offer new capabilities by introducing nonlinear optical or electrical materials into otherwise passive plasmonic waveguides²⁹. If the nonlinearities are strong enough, these devices can be made small compared with the characteristic decay lengths of SPPs and their performance parameters should not suffer from the unavoidable resistive losses in the metals.

While we have shown that weakly guided stripe waveguides cannot achieve deep subwavelength confinement, there exist alternative strongly guiding geometries that can provide markedly better confinement. This category of structures is of great interest for novel interconnection schemes. For example, Takahara and coworkers'

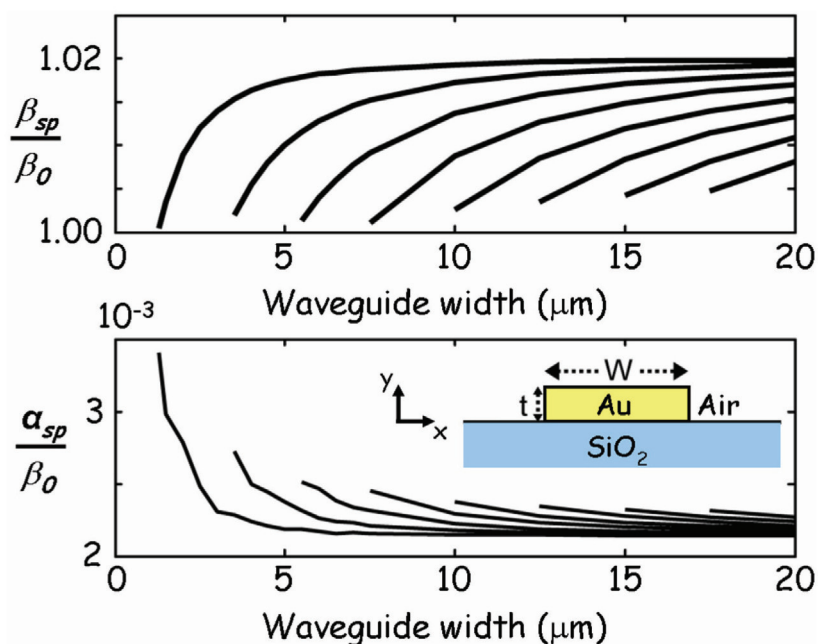


Fig. 5 Calculated complex propagation constants ($\beta_{sp} + i\alpha_{sp}$) for the eight lowest order leaky, quasi-TM SPP modes of varying width Au stripe waveguides. For these calculations, the Au stripe thickness was $t = 55$ nm and the free space excitation wavelength was $\lambda = 800$ nm. The magnitudes of β_{sp} and α_{sp} were normalized to the real part of the free space propagation constant β_0 . The inset shows the simulation geometry and the coordinate frame. (Reprinted with permission from²¹. © 2005 American Physical Society.)

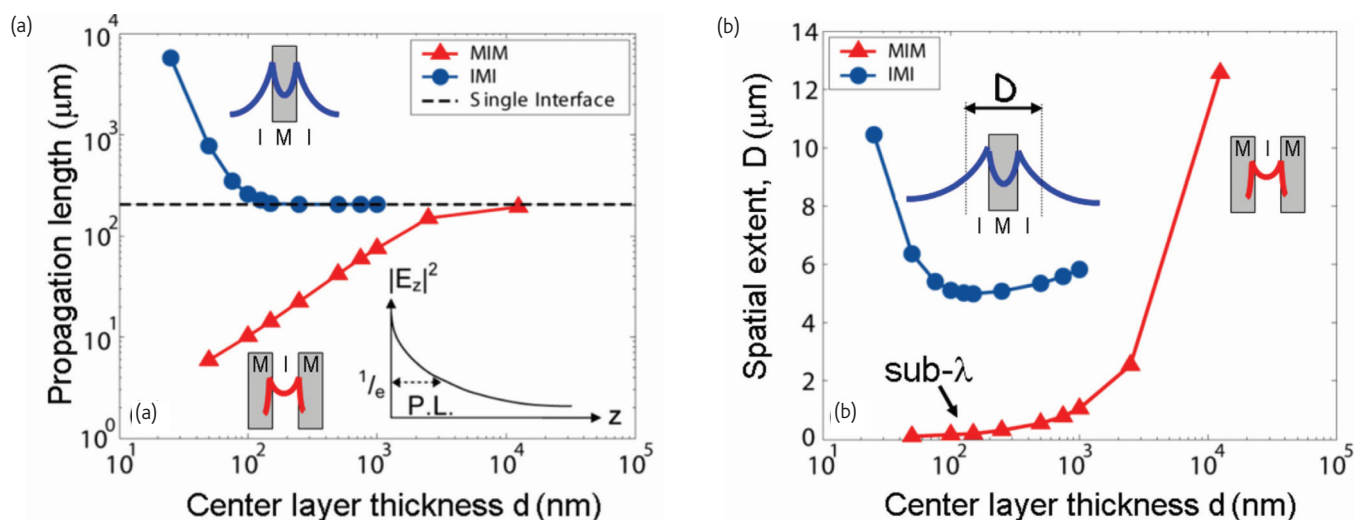


Fig. 6 Plot of (a) SPP propagation length and (b) spatial extent of the SPP modes as a function of the center-layer thickness for MIM and IMI plasmonic waveguides. The insets illustrate plotted terms. The reflection pole method was used for $\lambda = 1.55 \mu\text{m}$ with Au as the metal and air as the insulator. (Reprinted with permission from¹⁹. © 2004 The Optical Society of America.)

original paper on the SPP modes of a metal cylinder show that subwavelength mode diameters are possible and propagation over short distances can be realized¹². Waveguides consisting of two closely spaced metals also combine propagation distances of a few microns with deep-subwavelength confinement^{19,30,31}. Fig. 6a shows a comparison of propagation lengths (where the exponential decay in $|E_z|^2$ falls to the $1/e$ point) for planar metal/insulator/metal (MIM) waveguides and waveguides consisting of a metal film sandwiched between two insulators (IMI waveguides). These calculations were performed using the well-established reflection pole method at the important telecommunications wavelength of $1.55 \mu\text{m}$ ³². This technique, based on transfer matrix formalism, monitors the phase of the reflection coefficient denominator, and can be used to give the complex propagation constants of both bound and leaky modes in lossy waveguides. We again used Au ($\epsilon_{\text{Au}} = -95.92 + 10.97i$ at $\lambda = 1.55 \mu\text{m}$) as the metal and air as the insulator²⁸.

For a sufficiently large center-layer thickness, the propagation lengths for these two types of waveguides converge to the propagation length found for a single interface (dashed line in Fig. 6a). This is reasonable since the SPP modes on the two metal surfaces decouple when the spacing between them becomes large. As the center layer thickness decreases and the SPPs at the two interfaces start to interact, the propagation length along MIM structures decreases while it increases along IMI structures. In fact, IMI waveguides can reach centimeter propagation distances for very thin metal films. For obvious reasons, these are termed long-range SPP modes^{33,34}. These 'large' propagation distances can be understood by realizing that the spatial extent of the modes becomes as large as $10 \mu\text{m}$ at these extremely thin metallic film thicknesses (Fig. 6b). In this case, the SPP waves are

almost entirely propagating in the very low loss air region with very little field intensity inside the lossy (resistive) metal.

The MIM modes exhibit a continuous decrease in the propagation length as the center insulating layer thickness is reduced. However, Fig. 6b shows that by 'pushing' the metals closer together it is feasible to realize deep subwavelength mode diameters without running into problems with cutoff. For example, the spatial extent decreases to about 100 nm ($< \lambda/15$) for a metal-to-metal spacing of 50 nm . It seems possible, therefore, that information can be transported in a deep-subwavelength mode over short ($\sim 1 \mu\text{m}$) distances, which is impossible with conventional dielectric components. For CMOS-compatible Cu and Al plasmonic waveguides, similar numbers are found and are discussed in a recent publication¹⁹. Within short propagation distances, MIM structures also allow routing of electromagnetic energy around sharp corners and signals to be split in T-junctions³⁵. These unique features can be used to realize truly nanoscale photonic functionality and circuitry^{36,37}, although the maximum size of such circuits will be limited by the SPP propagation length. It is important to realize that for every type of waveguide, there is a clear, but different, trade-off between confinement and propagation distance (loss). The use of one type of waveguide over another will thus depend on application-specific constraints.

Plasmonics can bridge microscale photonics and nanoscale electronics

Based on the data presented above, it seems that the propagation lengths for plasmonic waveguides are too short to propagate SPPs with high confinement over the length of an entire chip ($\sim 1 \text{ cm}$). Although the manufacturability of long-range SPP waveguides may well be

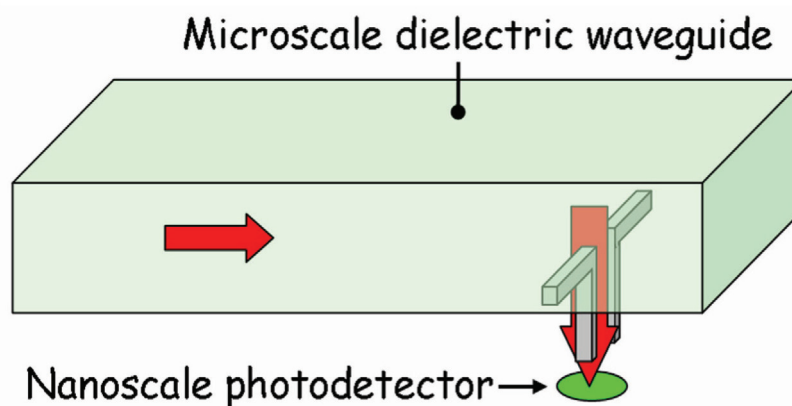


Fig. 7 Schematic of how a nanoscale antenna structure can serve as a bridge between microscale dielectric components and nanoscale electronic devices.

straightforward within a CMOS foundry, it is unlikely that such waveguides will be able to compete with well-established, low-loss, high-confinement Si, Si₃N₄, or other dielectric waveguides³⁸⁻⁴⁰. However, it is possible to create new capabilities by capitalizing on an additional strongpoint of metallic nanostructures. Metal nanostructures have a unique ability to concentrate light into nanoscale volumes. This capability has been employed to enhance a diversity of nonlinear optical phenomena. For example, surface-enhanced Raman scattering (SERS) is widely used in the field of biology⁴¹⁻⁴⁴. This technique makes use of the enhanced electromagnetic fields near metallic nanostructures to study the structure and composition of organic and biological materials. Enhancement factors on the order of 100 have been predicted and observed for spherical particles. Even greater enhancements can be obtained near carefully engineered metal optical antenna structures that basically resemble scaled-down versions of a car antenna⁴⁵. Recently, such antennas have even enabled single-molecule studies by SERS and white-light supercontinuum generation⁴⁶⁻⁴⁸.

Despite the numerous studies on antennas in the microwave and optical regimes, their application to solve current issues in chip-scale interconnection has remained largely unexplored. The field-concentrating abilities of optical antennas may serve to bridge the large gap between microscale dielectric photonic devices and nanoscale electronics (Fig. 7). This diagram shows a detail of a chip on which optical signals are routed through conventional dielectric optical waveguides. The mode size of such waveguides is typically one or two orders of magnitude larger than the underlying CMOS electronics. An antenna can be used to concentrate the electromagnetic signals from the waveguide mode into a deep subwavelength metal/insulator/metal waveguide and inject it into a nanoscale photodetector. The small size of the detector ensures a small capacitance, low-noise, and high-speed operation. By using metallic nanostructures as a bridge between photonics and electronics, we play to the strengths of metallic nanostructures (concentrating fields and subwavelength guiding), dielectric waveguides (low-loss information transport), and nanoscale electronic components (high-speed information processing).

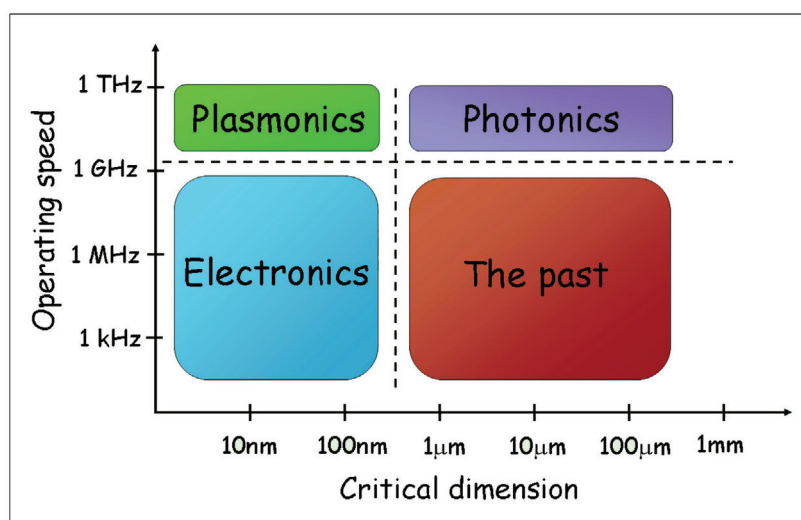


Fig. 8 Operating speeds and critical dimensions of various chip-scale device technologies, highlighting the strengths of the different technologies.

Conclusions

Plasmonics has the potential to play a unique and important role in enhancing the processing speed of future integrated circuits. The field has witnessed an explosive growth over the last few years and our knowledge base in plasmonics is rapidly expanding. As a result, the role of plasmonic devices on a chip is also becoming more well-defined and is captured in Fig. 8. This graph shows the operating speeds and critical dimensions of different chip-scale device technologies. In the past, devices were relatively slow and bulky. The semiconductor industry has performed an incredible job in scaling electronic devices to nanoscale dimensions. Unfortunately, interconnect delay time issues provide significant challenges toward the realization of purely electronic circuits operating above ~10 GHz. In stark contrast, photonic devices possess an enormous data-carrying capacity (bandwidth). Unfortunately, dielectric photonic components are limited in their size by the laws of diffraction, preventing the same scaling as in electronics. Finally, plasmonics offers precisely what electronics and photonics do not have:

the size of electronics and the speed of photonics. Plasmonic devices, therefore, might interface naturally with similar speed photonic devices and similar size electronic components. For these reasons, plasmonics may well serve as the missing link between the two device technologies that currently have a difficult time communicating. By increasing the synergy between these technologies, plasmonics may be able to unleash the full potential of nanoscale functionality and become the next wave of chip-scale technology. 

Acknowledgments

The authors would like to thank Rohan Kekatpure, Shanhui Fan, David Miller, Gernot Pomrenke, and Jung Shin for valuable discussions on the use of plasmonics to bridge the gap between microscale photonics and nanoscale electronics. This work was supported by a US Department of Defense Multidisciplinary University Research Initiative sponsored by the Air Force Office of Scientific Research (F49550-04-1-0437), a US National Science Foundation (NSF) Career Award (ECS-0348800), the Center for Probing the Nanoscale, an NSF Nanoscale Science and Engineering Center (PHY-0425897), and Intel.

REFERENCES

- Bohr, M. T., *Tech. Dig. IEDM* (1995), 241
- Chiang, T.-Y., et al., Impact of joule heating on scaling of deep sub-micron Cu/low-*k* interconnects. *IEEE Symp. VLSI Circuits, Dig. Tech. Papers* (2002), 38
- Banerjee, K., et al., *Tech. Dig. IEDM* (1996), 65
- Miller, D. A. B., *Proc. IEEE* (2000) **88**, 728
- Chen, G., et al., Predictions of CMOS compatible on-chip optical interconnect, *Int. Workshop System Level Interconnect Prediction*, (2005), 13
- Barnes, W. L., et al., *Nature* (2003) **424**, 824
- Takahara, J., and Kobayashi, T., *Opt. Photonics News* (2004) **15** (10), 54
- Brongersma, M. L., et al., *Mater. Res. Soc. Symp. Proc.* (1999) **502**, H10.5. [This reference contains the first occurrence of the word 'plasmonics' in title, subject, or abstract in the Inspec® database.]
- Economou, E. N., *Phys. Rev.* (1969) **182**, 539
- Raether, H., *Surface plasmons on smooth and rough surfaces and on gratings*, Springer-Verlag, New York, (1988)
- Burke, J. J., et al., *Phys. Rev. B* (1986) **33**, 5186
- Takahara, J., et al., *Opt. Lett.* (1997) **22**, 475
- Nikolajsen, T., et al., *Opt. Commun.* (2005) **244**, 455
- Reddick, R. C., et al., *Phys. Rev. B* (1989) **39**, 767
- Weeber, J.-C., et al., *Phys. Rev. B* (2001) **64**, 045411
- Weeber, J.-C., et al., *Phys. Rev. B* (2003) **68**, 115401
- Krenn, J. R., et al., *Europhys. Lett.* (2002) **60**, 663
- Kretschmann, E., *Z. Phys. A: Atoms Nucl.* (1971) **241**, 313
- Zia, R., et al., *J. Opt. Soc. Am. A* (2004) **21**, 2442
- Lamprecht, B., et al., *Appl. Phys. Lett.* (2001) **79**, 51
- Zia, R., et al., *Phys. Rev. B* (2005) **71**, 165431
- Zia, R., et al., *Opt. Lett.* (2005) **30**, 1473
- Zia, R., et al., unpublished results
- Al-Bader, S. J., *IEEE J. Quantum Electron.* (2004) **40**, 325
- Berini, P., *Phys. Rev. B* (2000) **61**, 10484
- Berini, P., *Phys. Rev. B* (2001) **63**, 125417
- Lusse, P., et al., *J. Lightwave Technol.* (1994) **12**, 487
- Palik, E. D., *Handbook of Optical Constants of Solids*, Academic Press, Orlando, FL, (1985) **18**, 804
- Krasavin, A.V., and Zheludev, N. I., *Appl. Phys. Lett.* (2004) **84**, 1416
- Bozhevolnyi, S. I., et al., *Phys. Rev. Lett.* (2005) **95**, 046802
- Veronis, G., and Fan, S., *Opt. Lett.* (2005) **30**, 3359
- Anemogiannis, E., et al., *J. Lightwave Technol.* (1999) **17**, 929
- Sarid, D., *Phys. Rev. Lett.* (1981) **47**, 1927
- Yang, F., et al., *Phys. Rev. Lett.* (1991) **66**, 2030
- Veronis, G., and Fan, S., *Appl. Phys. Lett.* (2005) **87**, 131102
- Tanaka, K., and Tanaka, M., *Appl. Phys. Lett.* (2003) **82**, 1158
- Bozhevolnyi, S. I., et al., *Nature* (2006) **440**, 508
- Lee, K. K., et al., *Opt. Lett.* (2001) **26**, 1888
- Daldosso, N., et al., *J. Lightwave Technol.* (2004) **22**, 1734
- Sparacin, D. K., et al., *J. Lightwave Technol.* (2005) **23**, 2455
- Félijd, N., et al., *Appl. Phys. Lett.* (2003) **82**, 3095
- Shafer-Peltier, K. E., et al., *J. Am. Chem. Soc.* (2003) **125**, 588
- Haynes, C. L., and Van Duyne, R. P., *J. Phys. Chem. B* (2003) **107**, 7426
- Drachev, V. P., et al., *J. Phys. Chem. B* (2004) **108**, 18046
- Crozier, K. B., et al., *J. Appl. Phys.* (2003) **94**, 4632
- Nie, S. M., and Emery, S. R., *Science* (1997) **275**, 1102
- Kneipp, K., et al., *Phys. Rev. Lett.* (1997) **78**, 1667
- Fromm, D. P., et al., *J. Chem. Phys.* (2006) **124**, 061101